Japanese Journal of Applied Physics **53**, 04ER05 (2014) **REGULAR PAPER**
http://dx.doi.org/10.7567/JJAP.53.04ER05

Surface-activated-bonding-based InGaP-on-Si double-junction cells

Naoteru Shigekawa[1,2*], Masashi Morimoto[1], Shota Nishida[1], and Jianbo Liang[1,2]

[1]*Graduate School of Engineering, Osaka City University, Osaka 558-8585, Japan*
[2]*JST/CREST, Osaka 558-8585, Japan*
E-mail: shigekawa@elec.eng.osaka-cu.ac.jp

Received September 24, 2013; accepted November 5, 2013; published online February 7, 2014

InGaP-on-Si double-junction cells were fabricated by the surface activated bonding of InGaP-based top cell layers grown on GaAs substrates to Si-based bottom cells and the selective etching of GaAs substrates. The open-circuit voltage of the double-junction cells in the tandem operation was close to the sum of the open-circuit voltages of the top and bottom cells. The efficiency in the tandem operation of the n-on-p InGaP/(100)-Si double-junction cells was higher than the efficiencies of the respective subcells. © 2014 The Japan Society of Applied Physics

1. Introduction

Tandem solar cells composed of stacks of group-III–arsenide- or phosphide-based subcells with different band gaps[1–7] are promising candidates for the third-generation solar cells[8] and have reportedly shown the highest conversion efficiencies among a variety of solar cell structures.[9] For metal organic chemical vapor deposition (MOCVD)-grown InGaP/InGaAs/Ge tandem cells,[6] which have a typical tandem cell structure, a conversion efficiency greater than 30% was reported. Efficiencies were increased by concentrating solar light on cells with smaller areas, i.e., by employing the concentrating photovoltaic (CPV) approach.[10,11]

Higher efficiencies in the tandem cells can be achieved by increasing the number of subcells or by decreasing the thermal dissipation of energy absorbed in each subcell.[8] In this scheme, the combination of their band gaps must be selected so that the currents due to photons absorbed in the respective subcells are equal to one another, or the current-matching condition must be fulfilled. Furthermore, Ge-based bottom cells in the above structures should preferably be replaced with Si-based ones from a practical viewpoint since Si is the most widely used semiconductor material in the solar cell industry. Thus, group-III–arsenides or phosphides/Si junctions are likely to be the ideal structure for tandem cells.

The majority of previously reported tandem cells were fabricated by growing the entire semiconductor-layer structure on substrates or through the monolithic approach. The growth of compound-semiconductor-based cells on Si substrates or on Si-based bottom cells was reported.[12–14] It is difficult, however, to prepare tandem cells with a larger number of subcells on Si substrates in a similar way because (1) the lattice constants and thermal expansion coefficients of semiconductor materials for the respective subcells are likely to be different from each other and (2) the anti phase domains often appear in layers of group-III–arsenides or phosphides grown on Si substrates.[15]

Tandem cells can alternatively be fabricated by bonding subcells or using the hybrid approach.[16–18] In conventional bonding, the surfaces of samples must be carefully treated prior to the bonding and samples must be heated when bonding them in order to achieve bonding interfaces with excellent electrical characteristics,[16,19] which are essentially required to achieve high efficiencies.

Surface-activated bonding (SAB), in which samples are bonded to each other after their surfaces are activated by Ar plasma irradiation,[20–25] has enabled us to fabricate semiconductor junctions without heating samples.[20] Consequently, junctions of dissimilar materials with different thermal expansion coefficients can be made by SAB. The structural properties of Si/Si junctions were previously observed.[21,22] The current–voltage (I–V) characteristics of SAB-based Si/Si, Si/GaAs, Si/InP, and Si/GaN junctions were reported.[23,24,26]

We investigated the electrical properties of SAB-based Si/GaAs junctions by measuring their I–V and capacitance–voltage characteristics.[27] We successfully bonded the backsides of nitride-based cells fabricated on GaN substrates were successfully bonded to epitaxially grown InGaP cell structures by SAB so that nitride/InGaP-double-junction cells were formed.[28] We also measured the I–V characteristics of p–n junctions fabricated from a variety of semiconductor layers with different doping concentrations.[29] We found that the resistance across the bonding interface $R_{\mathrm{interface}}$ decreased as the concentrations of impurities in p- and n-doped layers increased. The lowest $R_{\mathrm{interface}}$ that we obtained was $0.13\,\Omega\cdot\mathrm{cm}^2$.

In this work, as the first step in realizing group-III–arsenide- or phosphide-on-Si multi-junction cells, we fabricated n-on-p InGaP/(100)-Si, p-on-n InGaP/(100)-Si, and p-on-n InGaP/(111)-Si double-junction cells by attaching InGaP-based top cells to Si-based bottom cells by SAB. We measured their I–V characteristics and examined the relationship between the characteristics of the double-junction cells in the tandem operation and those of the constituent subcells in order to discuss the feasibility of SAB.

2. Experimental procedure and results

2.1 Tandem cell fabrication

We prepared n-on-p (100) Si-based bottom cell structures by the ion implantation of phosphorus atoms to high-resistivity ($10.9\,\Omega\cdot\mathrm{cm}$) p-type (100) Si substrates and the subsequent rapid thermal annealing. The dose and acceleration energy used in the ion implantation were $4.3 \times 10^4\,\mathrm{cm}^{-2}$ and 10 keV, respectively. The temperature and duration of the annealing were 900 °C and 1 min, respectively. Preparatory measurements using SIMS suggested that the distribution of the concentration of phosphorus atoms revealed a peak with a height of $6 \times 10^9\,\mathrm{cm}^{-3}$ at a depth of 12 nm after the annealing. We also formed p^+ layers by the ion implantation of boron atoms and annealing in order to obtain good ohmic contacts on the backsides of the bottom cells. The dose and

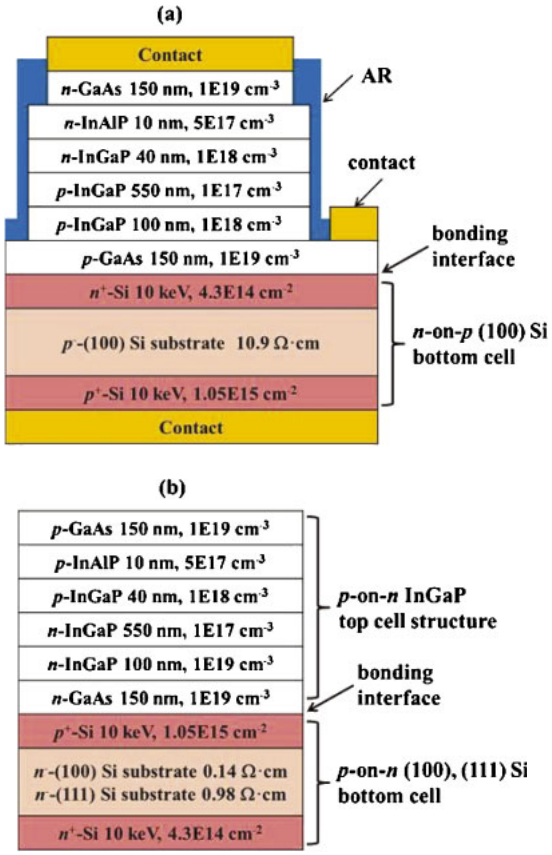

Fig. 1. (Color online) (a) Schematic cross section of an n-on-p InGaP/(100)-Si double-junction cell. (b) Semiconductor-layer structures of p-on-n InGaP/(100)-Si and p-on-n InGaP/(111)-Si double-junction cells.

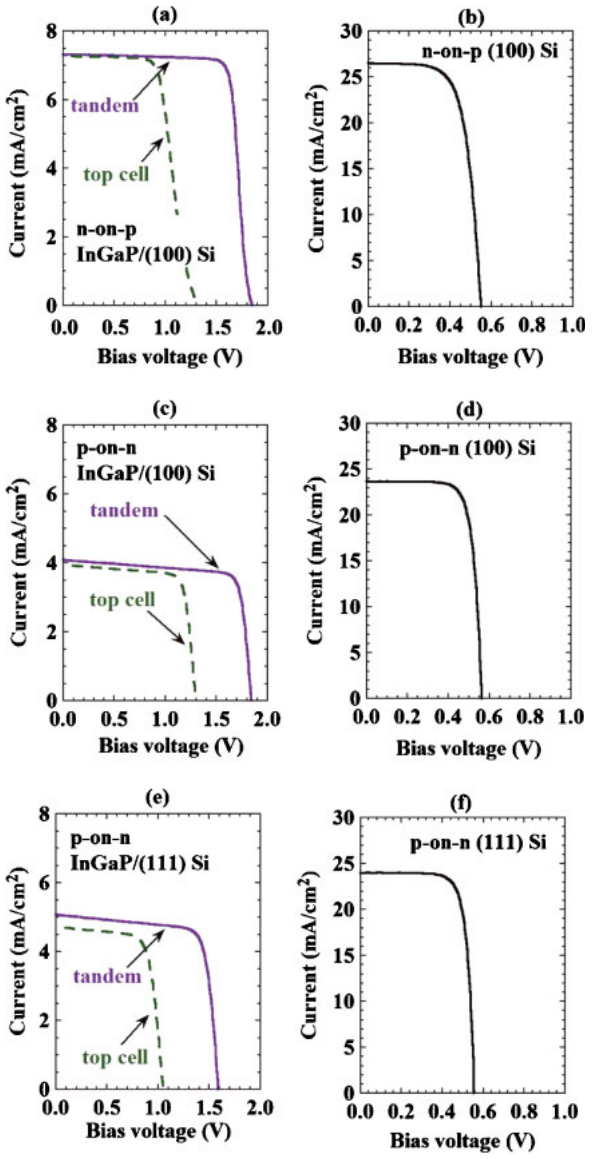

Fig. 2. (Color online) *I–V* characteristics of (a) an n-on-p InGaP/(100)-Si double-junction cell, (b) an n-on-p (100)-Si-based bottom cell, (c) a p-on-n InGaP/(100)-Si double-junction cell, (d) a p-on-n (100)-Si-based bottom cell, (e) a p-on-n InGaP/(111)-Si double-junction cell, and (f) a p-on-n (111)-Si-based bottom cell measured at room temperature under the conditions of air mass 1.5 G and one sun.

acceleration energy were $1.05 \times 10^{15}\,\mathrm{cm}^{-2}$ and 10 keV, respectively. We estimated that the distribution of the concentration of boron atoms revealed a peak with a height of $1.4 \times 10^{20}\,\mathrm{cm}^{-3}$ at a depth of 50 nm after the annealing.

The lattice-matched n-on-p InGaP top cell structures were obtained by the MOCVD growth of the etch stopper layer, top-cell structure, and contact layer on (100) GaAs substrates. The contact layer of the top cell structures was bonded to the bottom cell structures by SAB. After the GaAs substrates were selectively etched off, n-on-p InGaP/(100)-Si double junction cells were fabricated using a conventional device process sequence, i.e., by the selective etching of the etch stopper layers, the mesa etching of the top cell, the formation of contacts, and the deposition of an anti reflection film.

The schematic cross section of the double-junction cell is shown in Fig. 1(a). The constituent n-on-p InGaP top cells, which were composed of an n^+-doped GaAs emitter contact layer (150 nm, $1 \times 10^{19}\,\mathrm{cm}^{-3}$), an n-doped InAlP window layer (10 nm, $\sim 5 \times 10^{17}\,\mathrm{cm}^{-3}$), an n-doped InGaP emitter layer (40 nm, $\sim 1 \times 10^{18}\,\mathrm{cm}^{-3}$), a p-doped InGaP photo absorption layer (550 nm, $\sim 1 \times 10^{17}\,\mathrm{cm}^{-3}$), and a p^+-doped InGaP back-surface field layer (100 nm, $\sim 1 \times 10^{18}\,\mathrm{cm}^{-3}$), were placed on a p^+-doped GaAs contact layer (150 nm, $\sim 1 \times 10^{19}\,\mathrm{cm}^{-3}$). The emitter and base contacts for the top cells and the base contacts for the bottom cells were fabricated by evaporating Ti/Au and Al, respectively, without alloying. The area of the emitter mesa of the top cells was 1-by-1 mm^2. The width and pitch of the emitter grids were 10 and 100 μm, respectively. Note that the characteristics of the top cells as part of the double-junction cells are measurable by probing the contacts formed on the exposed base layers. We fabricated p-on-n InGaP/(100)-Si and p-on-n InGaP/(111)-Si double-junction cells in a similar manner. Their semiconductor-layer structures are shown in Fig. 1(b).

2.2 Cell characterization

The *I–V* characteristics of the respective cells were measured using an in-house solar simulator under the conditions of air mass 1.5 G and one sun at room temperature. The *I–V* characteristics of the n-on-p InGaP/(100)-Si double-junction cell are shown in Fig. 2(a). The characteristics observed in the tandem operation and those of the top cell are shown in the figure. Figure 2(b) shows the *I–V* characteristics of the

Table I. Parameters extracted from the respective cell characteristics.

n-on-p InGaP/(100)-Si double-junction cell

Parameter	Tandem	Top cell	Bottom cell
V_{OC} (V)	1.85	1.32	0.55
J_{SC} (mA/cm^2)	7.31	7.26	26.50
FF (%)	82.1	65.6	68.1
Efficiency (%)	11.1	6.3	9.9
Series resistance (Ω·cm^2)	98	183	2.9
Shunt resistance (Ω·cm^2)	$\sim 2 \times 10^4$	$\sim 2 \times 10^4$	$\sim 3 \times 10^3$

p-on-n InGaP/(100)-Si double-junction cell

Parameter	Tandem	Top cell	Bottom cell
V_{OC} (V)	1.84	1.30	0.56
J_{SC} (mA/cm^2)	4.08	3.94	23.66
FF (%)	79.4	78.0	76.8
Efficiency (%)	6.0	4.0	10.2
Series resistance (Ω·cm^2)	26	34	1.8
Shunt resistance (Ω·cm^2)	$\sim 4 \times 10^3$	$\sim 4 \times 10^3$	$> 1 \times 10^4$

p-on-n InGaP/(111)-Si double-junction cell

Parameter	Tandem	Top cell	Bottom cell
V_{OC} (V)	1.59	1.05	0.56
J_{SC} (mA/cm^2)	5.07	4.72	23.97
FF (%)	77.0	72.9	77.8
Efficiency (%)	6.2	3.6	10.4
Series resistance (Ω·cm^2)	22	26	1.6
Shunt resistance (Ω·cm^2)	$\sim 3 \times 10^3$	$\sim 4 \times 10^3$	$> 1 \times 10^4$

independently fabricated n-on-p (100)-Si-based bottom cell. Figures 2(c) and 2(d) the show results for the p-on-n InGaP/(100)-Si double-junction cell and bottom cell, respectively. Results for the p-on-n InGaP/(111)-Si double-junction cell and bottom cell are shown in Figs. 2(e) and 2(f), respectively. The series and shunt resistances were simply estimated by numerically calculating dI/dV under the zero-current and zero-voltage conditions, respectively, for the respective *I–V* characteristics.

The values of the parameters extracted from the respective *I–V* characteristics are shown in Table I, from which we obtained the following findings:

(1) In the n-on-p InGaP/(100)-Si double-junction cell, the open-circuit voltage in the tandem-cell operation, $V_{OC,tandem}$ (1.85 V), is almost in agreement with the sum of the open-circuit voltage of the top cell, $V_{OC,top}$ (1.32 V), and that of the bottom cell, $V_{OC,bottom}$ (0.55 V). Similar results are also obtained for the other double-junction cells.

(2) In each double-junction cell, the short-circuit current in the tandem operation, $J_{SC,tandem}$, is slightly larger than that in the top cell, $J_{SC,top}$. In contrast, $J_{SC,tandem}$ is much smaller than the short-circuit current in the bottom cell, $J_{SC,bottom}$. In the n-on-p InGaP/(100)-Si double-junction cell, for example, $J_{SC,tandem}$ and $J_{SC,top}$ are 7.31 and 7.26 mA/cm^2, respectively, both of which are smaller than $J_{SC,bottom}$ (26.50 mA/cm^2).

(3) The difference between $J_{SC,tandem}$ and $J_{SC,top}$ is the largest for the p-on-n InGaP/(111)-Si double-junction cell ($5.07 - 4.72 = 0.35$ mA/cm^2). The difference is the smallest for the n-on-p InGaP/(100)-Si double-junction cell (≈ 0.05 mA/cm^2).

(4) The series resistance in the tandem operation, $R_{ser,tandem}$, is slightly smaller than the series resistance in the top cell, $R_{ser,top}$. In contrast, $R_{ser,tandem}$ is larger than that in the bottom cell, $R_{ser,bottom}$. In addition, $R_{ser,tandem}$ is much larger than $R_{interface}$ (≈ 0.1–0.2 Ω·cm^2).[29] Typically for the n-on-p InGaP/(100)-Si double-junction cell, $R_{ser,tandem}$, $R_{ser,top}$, and $R_{ser,bottom}$ are 98, 183, and 2.9 Ω·cm^2, respectively.

(5) The fill factor in the tandem operation, FF_{tandem}, is larger than that of the top cell, FF_{top}.

(6) The efficiency of the n-on-p InGaP/(100)-Si double-junction cell in the tandem operation (11.1%) is higher than that of the p-on-n double-junction cells (6.0–6.2%). Similarly, the efficiency of the top cell in the n-on-p InGaP/(100)-Si double-junction cell (6.3%) is higher that in the p-on-n double-junction cells (3.6–4.0%). Furthermore, in the n-on-p InGaP/(100)-Si double-junction cell, the efficiency in the tandem operation is higher than those of the constituent top and bottom cells. In each of the two p-on-n double-junction cells, the efficiency in the tandem operation is higher than that of the top cell but lower than that of the bottom cell.

(7) $J_{SC,top}$ in the n-on-p double-junction cell (7.26 mA/cm^2) is larger than $J_{SC,top}$'s in the p-on-n double-junction cells (3.94 and 4.72 mA/cm^2).

3. Discussion

The finding that $R_{ser,tandem}$ in each double-junction cell is much larger than $R_{interface}$ [finding (4) mentioned above] suggests that the dominant factor determining the series resistance in the tandem operation is the resistance at contacts, which is possibly the resistance at the grid-shaped emitter contacts of the top cell. Note that the contacts were made through the non-alloy process. The fact that $R_{ser,top}$ is higher than $R_{ser,tandem}$ can be explained from this viewpoint since the resistance at the base contact of the top cell, which was also formed through the non-alloy process, as well as the internal resistance in the doped base layer are assumed to additively contribute to $R_{ser,top}$. The difference between FF_{tandem} and FF_{top} [finding (5)] is also related to the result that $R_{ser,top}$ is larger than $R_{ser,tandem}$.

The values of $R_{ser,tandem}$ observed in the present work are much larger than the series resistance in the well-established triple-junction cells applied to CPV, which is reportedly ≈ 0.02 Ω·cm^2.[6,11] A lower series resistance might be obtained by optimizing the formation of ohmic contacts and making bonding interfaces of more highly doped layers.

The observation for short-circuit currents that $J_{SC,top} < J_{SC,tandem} \ll J_{SC,bottom}$ [finding (2)] implies that the performance in the tandem operation is limited by the characteristics of the top cell. The higher efficiency in the tandem operation in the n-on-p double-junction cell than in the p-on-n double-junction cells [finding (6)] is, consequently, attributable to the difference in $J_{SC,top}$ between the n-on-p and p-on-n top cells [finding (7)]. Given that the short-circuit current in InGaP-based cells strongly depends on the thickness of the absorption layer up to 1 μm,[30] the difference in $J_{SC,top}$ between the n-on-p and p-on-n top cells might be attributable to uncontrolled fluctuations in the thickness of the InGaP absorption layer (nominally 0.55 μm). The difference in $J_{SC,top}$ could also be explained by the valence-band offset of InAlP/InGaP interfaces, which is reportedly larger than the

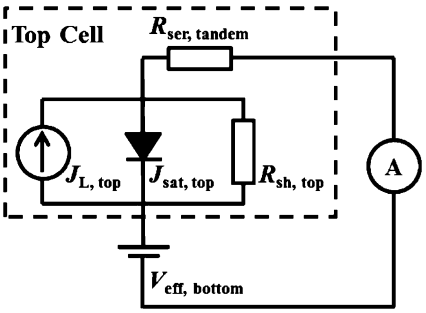

Fig. 3. Equivalent circuit of the double-junction cells in the short-circuit tandem operation.

conduction-band offset.[31] In either case, the efficiencies in the top cells hence those in the double-junction cells in the tandem operation are likely to be increased by revising the layer structure in the top cells.

The equivalent circuit of the double-junction cell in the short-circuit tandem operation is shown in Fig. 3. The top cell in the equivalent circuit is composed of a current source due to the solar light illumination ($J_{L,top}$ in the figure), a p–n diode with the saturation current $J_{sat,top}$, and $R_{sh,top}$, which are connected parallel to each other. The fact that $J_{SC,top} \ll J_{SC,bottom}$ means that, in such operation modes, the bottom cell is effectively replaced with a voltage source, $V_{eff,bottom}$, whose magnitude is close to $V_{OC,bottom}$. $V_{eff,bottom}$ is likely to induce changes in both of the currents flowing through the p–n diode and $R_{sh,top}$ in the top cell, which are assumed to bring about $J_{SC,tandem}$ larger than $J_{SC,top}$. The most marked increase in J_{SC} in the p-on-n InGaP/(111)-Si double-junction cell among the fabricated double-junction cells [finding (3)] is quantitatively explained by the lowest $V_{OC,top}$, which suggests that $J_{sat,top}$ is the largest, and the smallest $R_{sh,top}$ in this cell.

The result that $V_{OC,tandem} \approx V_{OC,top} + V_{OC,bottom}$ in each double-junction cell [finding (1)] indicates that the top and bottom cells are electrically connected. Also noting that even double-junction cells composed of InGaP-based top cells grown on (100) GaAs substrates and (111)-Si-based bottom cells normally operate as tandem cells in spite of the difference in the crystal symmetries in the bonding layers, the surface-activated bonding is assumed to be promising as a practical method of fabricating hybrid tandem cells with high efficiencies, although the fundamental properties of the bonding interfaces as well as the mechanism inducing an electrical conduction across the interfaces are not yet completely understood.

4. Conclusion

We fabricated three types of InGaP/Si double-junction solar cells by attaching InGaP-based top-cell layers grown on GaAs substrates to Si-based bottom-cell structures and selectively etching off the GaAs substrates. In each double-junction cell, the open-circuit voltage in the tandem operation was almost in agreement with the sum of the open-circuit voltages of the top and bottom subcells. The magnitude of the difference between the short-circuit currents in the tandem operation and top cell, which was the largest in the p-on-n InGaP/(111)-Si double-junction cell, might be explained in reference to the equivalent circuit of the double-junction cells. In the n-on-p InGaP/(100)-Si double-junction cell, an efficiency of 11.1% was attained in the tandem operation, which was larger than the efficiencies of the top and bottom cells. Higher efficiencies in the tandem operation are assumed to be achieved by revising the layer structures of the top cells and the process for fabricating contacts, which are likely to increase the short-circuit current of the top cells and decrease the series resistance.

1) H. Sugiura, C. Amano, A. Yamamoto, and M. Yamaguchi, Jpn. J. Appl. Phys. **27**, 269 (1988).
2) J. M. Olson, S. R. Kurtz, A. E. Kibbler, and P. Faine, Appl. Phys. Lett. **56**, 623 (1990).
3) K. A. Bertness, S. R. Kurtz, D. J. Friedman, A. E. Kibbler, C. Kramer, and J. M. Olson, Appl. Phys. Lett. **65**, 989 (1994).
4) T. Takamoto, E. Ikeda, H. Kurita, and M. Ohmori, Appl. Phys. Lett. **70**, 381 (1997).
5) T. Takamoto, E. Ikeda, H. Kurita, M. Ohmori, M. Yamaguchi, and M.-J. Yang, Jpn. J. Appl. Phys. **36**, 6215 (1997).
6) T. Takamoto, M. Kaneiwa, M. Imaizumi, and M. Yamaguchi, Prog. Photovoltaics **13**, 495 (2005).
7) J. F. Geisz, S. Kurtz, M. W. Wanlass, J. S. Ward, A. Duda, D. J. Friedman, J. M. Olson, W. E. McMahon, T. E. Moriarty, and J. T. Kiehl, Appl. Phys. Lett. **91**, 023502 (2007).
8) M. A. Green, Prog. Photovoltaics **9**, 123 (2001).
9) Web [http://www.nrel.gov/ncpv/images/efficiency_chart.jpg].
10) M. Yamaguchi and A. Luque, IEEE Trans. Electron Devices **46**, 2139 (1999).
11) K. Nishioka, T. Takamoto, T. Agui, M. Kaneiwa, Y. Uraoka, and T. Fuyuki, Sol. Energy Mater. Sol. Cells **90**, 1308 (2006).
12) T. Soga, K. Baskar, T. Kato, T. Jimbo, and M. Umeno, J. Cryst. Growth **174**, 579 (1997).
13) M. R. Lueck, C. L. Andre, A. J. Pitera, M. L. Lee, E. A. Fitzgerald, and S. A. Ringel, IEEE Electron Device Lett. **27**, 142 (2006).
14) M. J. Archer, D. C. Law, S. Mesropian, M. Haddad, C. M. Fetzer, A. C. Ackerman, C. Ladous, R. R. King, and H. A. Atwater, Appl. Phys. Lett. **92**, 103503 (2008).
15) Ph. Komninou, J. Stoemenos, G. P. Dimitrakopulos, and Th. Karakostas, J. Appl. Phys. **75**, 143 (1994).
16) K. Tanabe, A. F. i. Morral, H. A. Atwater, D. J. Aiken, and M. W. Wanlass, Appl. Phys. Lett. **89**, 102106 (2006).
17) K. Tanabe, K. Watanabe, and Y. Arakawa, Sci. Rep. **2**, 349 (2012).
18) H. Mizuno, K. Makita, and K. Matsubara, Appl. Phys. Lett. **101**, 191111 (2012).
19) M. J. Jackson, B. L. Jackson, and M. S. Goorsky, J. Appl. Phys. **110**, 104903 (2011).
20) H. Takagi, K. Kikuchi, R. Maeda, T. R. Chung, and T. Suga, Appl. Phys. Lett. **68**, 2222 (1996).
21) H. Takagi, R. Maeda, T. R. Chung, N. Hosoda, and T. Suga, Jpn. J. Appl. Phys. **37**, 4197 (1998).
22) H. Takagi, R. Maeda, N. Hosoda, and T. Suga, Jpn. J. Appl. Phys. **38**, 1589 (1999).
23) M. M. R. Howlader, T. Watanabe, and T. Suga, J. Vac. Sci. Technol. B **19**, 2114 (2001).
24) M. M. R. Howlader, T. Watanabe, and T. Suga, J. Appl. Phys. **91**, 3062 (2002).
25) C. Wang, E. Higurashi, and T. Suga, Jpn. J. Appl. Phys. **47**, 2526 (2008).
26) N. Shigekawa, N. Watanabe, and E. Higurashi, Proc. 3rd Int. IEEE Workshop Low-Temperature Bonding for 3D Integration, 2012, p. 109.
27) J. Liang, T. Miyazaki, M. Morimoto, S. Nishida, N. Watanabe, and N. Shigekawa, Appl. Phys. Express **6**, 021801 (2013).
28) N. Shigekawa, J. Liang, and N. Watanabe, accepted for publication in Proc. 39th IEEE Photovoltaic Specialists Conf.
29) J. Liang, S. Nishida, M. Morimoto, and N. Shigekawa, Electron. Lett. **49**, 830 (2013).
30) T. Takamoto, E. Ikeda, H. Kurita, and M. Ohmori, Sol. Energy Mater. Sol. Cells **35**, 25 (1994).
31) X. H. Zhang, S. J. Chua, and W. J. Fan, Appl. Phys. Lett. **73**, 1098 (1998).